Communication in Physical Sciences, 2026, 13(2): 480-501

Adsorption Performance and Modelling of Cd^{2+} Ions Removal Using Pyrolysed Palm Kernel Shell

Idowu J. Esho*, Emmanuel F. Olasehinde and Matthew A. Adebayo*
Received: 28 December 2025/ Accepted: 11 March 2025/Published: 20 March 2026
https://dx.doi.org/10.4314/cps.v13i3.8

***Abstract*:** *Valorisation of agricultural waste into sustainable high-performance adsorbents offers a cost-effective pathway for heavy metal removal. This study reports the adsorption performance and mechanistic behaviour of cadmium(II) remediation employing raw and pyrolysed palm kernel shell (PPKS). Characterisation data of PPKS indicated substantiate functional groups at the surface, enhanced mesopore structure up to 112.91 m^2/g, and produced higher thermal stability, all of which were demonstrated by FTIR, BET, SEM–EDX, XRD, TGA, and zeta potential data. Batch adsorption experiments showed substantial pH-dependent adsorption, with higher removal efficiency of about 92% – 96% at pH 5 – pH 6. The maximum adsorption capacity increased from 72.1 mg/g (raw PKS) to 107.4 mg/g after pyrolysis. Adsorption kinetic data highlighted that the process occurs via multiple steps, which are best interpreted through the model by Avrami fractional order, while the Liu isotherm provided an excellent fit for the equilibrium data. Thermodynamic parameters emphasized spontaneous and endothermic adsorption with negative $\Delta G°$ and positive $\Delta H°$ values. These data present pyrolysed palm kernel shell (PPKS) as an efficient, low-cost, and circular-economy-compatible adsorbent for remediation of cadmium-contaminated water, offering practical insights for sustainable wastewater management. The Liu isotherm provided a better equilibrium fitting, while the adsorption kinetic study showed multiple steps that were best controlled by the model from Avrami fractional order. Based on the data obtained in this present study, pyrolysed palm kernel shell (PPKS) is an alternative and effective adsorbent for removal of cadmium from contaminated aquatic systems, and this offers important understanding for eco-friendly wastewater treatment methods.*

Keywords: *Palm-kernel shell, Cadmium(II), Kinetic modelling, Isotherm modelling, Thermodynamic analysis*

Idowu J. Esho*
Department of Chemistry, Federal College of Education (Special), Oyo, Nigeria)
Email: esho.idowu2627@fcesoyo.edu.ng
https://orcid.org/0000-0002-4231-808X

Emmanuel F. Olasehinde
Department of Chemistry, The Federal University of Technology, Akure, Nigeria
Email: feolasehinde@futa.edu.ng

Matthew A. Adebayo
Department of Chemistry, The Federal University of Technology, Akure, Nigeria
Email: adebayoma@futa.edu.ng
https://orcid.org/0000-0002-6009-4075

1.0 Introduction

Contamination of aquatic environments by heavy metals remains a significant global environmental and public health concern owing to their persistence, non-biodegradable nature, toxicity, and tendency to bioaccumulate in living organisms (Awaka-Ama *et al.,* 2024). Among toxic heavy metals, cadmium (Cd^{2+}) is particularly hazardous even at trace concentrations and has been associated with severe health effects including renal dysfunction, carcinogenicity, skeletal damage, and metabolic disorders (Ladan *et al*., 2026). Major anthropogenic sources of cadmium contamination include electroplating operations, battery manufacturing, pigment production, mining activities, and metallurgical industries, which frequently discharge

contaminated effluents into aquatic systems. Consequently, strict regulatory limits have been established for cadmium concentrations in potable water, highlighting the urgent need for efficient and sustainable wastewater treatment technologies (Yichuan *et al.,* 2025).

Conventional methods for Cd^{2+} removal from wastewater, such as chemical precipitation, ion exchange, membrane filtration, and electrochemical treatments, often suffer from high operational costs, complex infrastructure requirements, generation of secondary pollutants, and reduced efficiency at low metal concentrations. These limitations have stimulated increasing interest in adsorption technology, which is widely regarded as a flexible, cost-effective, and environmentally friendly alternative for heavy-metal remediation (Akpanudo & Chibuzo, 2020). Adsorption processes offer advantages including operational simplicity, high removal efficiency, and the possibility of adsorbent regeneration and reuse, making them attractive for large-scale environmental applications (Kumari *et al.,* 2025; Yichuan *et al.,* 2025).

In recent years, biomass-derived adsorbents and biochar materials have emerged as sustainable alternatives due to their abundant availability, porous structures, and diverse surface functional groups capable of interacting with metal ions. Agricultural wastes, in particular, provide low-cost precursors for producing carbonaceous adsorbents while simultaneously addressing waste management challenges. Studies have demonstrated the effectiveness of palm kernel shell charcoal for removing Pb^{2+} and Cd^{2+} ions from wastewater, with adsorption performance strongly influenced by operating parameters such as adsorbent dosage and contact time (Oluyemi *et al.,* 2012). Similarly, investigations using various agricultural biomasses—including cocoa husk, cassava peel, corn residues, and oil palm bagasse—have shown that Cd^{2+} adsorption primarily occurs through ion exchange and complexation with oxygen-containing functional groups such as hydroxyl and carboxyl groups (Villabona-Ortíz *et al.,* 2021).

Palm kernel shell (PKS), a major by-product of the palm oil industry, is generated in large quantities worldwide and represents an inexpensive and renewable precursor for adsorbent production. However, untreated PKS typically exhibits limited surface area and low adsorption efficiency due to insufficient pore development. Thermochemical treatments such as pyrolysis significantly enhance adsorption properties by increasing carbonisation, developing porous structures, and generating oxygen-containing functional groups that act as active adsorption sites. Residual charcoal derived from pyrolysed oil palm shells has demonstrated promising Cd^{2+} adsorption performance, with adsorption behaviour commonly described by Langmuir isotherm models under optimized operational conditions (Faisal *et al.,* 2022).

Recent advances further highlight the potential of oil palm waste–derived materials as high-performance adsorbents aligned with circular economy principles. Surface functionalization and activation treatments have been shown to substantially improve adsorption capacity, stability, and regeneration efficiency, enabling their integration into practical wastewater treatment systems (Mohd Hamzah *et al.,* 2025). Optimization strategies such as chemical modification and response surface methodology have also been employed to enhance cadmium adsorption efficiency in modified biochars by tailoring surface chemistry and pore structure (Ding *et al.,* 2023).

The adsorption performance of biomass-derived carbons is strongly governed by their physicochemical properties, including surface area, pore distribution, functional groups, and surface charge characteristics, all of which depend on preparation conditions such as

activation method and pyrolysis temperature. Adsorption mechanisms for Cd^{2+} typically involve electrostatic attraction, surface complexation, ion exchange, and interactions between metal ions and functional groups on carbon surfaces. Comparable adsorption investigations using engineered materials such as hydroxyapatite have demonstrated that adsorption behaviour can vary between physical and chemical mechanisms depending on adsorbent structure and surface chemistry (Ofudje *et al.,* 2023). Therefore, understanding the relationship between material structure and adsorption behaviour is essential for designing efficient adsorbents.

Adsorption studies commonly employ kinetic, equilibrium, and thermodynamic modelling to elucidate removal mechanisms. Kinetic models such as pseudo-first-order and pseudo-second-order equations provide insight into rate-controlling processes, while isotherm models including Langmuir, Freundlich, Temkin, and hybrid models describe adsorption capacity and surface heterogeneity. Thermodynamic parameters—Gibbs free energy, enthalpy, and entropy changes—further reveal the spontaneity and energetic nature of adsorption processes. Despite extensive research on biomass-based adsorbents, many studies report adsorption performance without adequately correlating adsorption modelling outcomes with detailed surface characterization and surface charge behaviour, which are critical for explaining adsorption mechanisms and pH-dependent uptake trends (Yichuan *et al.,* 2025). Although palm kernel shell–derived adsorbents have shown promising performance, systematic investigations linking physicochemical characteristics of pyrolysed palm kernel shell with adsorption modelling and mechanistic interpretation for Cd^{2+} removal remain limited. In particular, the influence of surface charge behaviour and adsorption site heterogeneity on cadmium uptake mechanisms requires further clarification.

Therefore, this study evaluates the adsorption performance and mechanistic behaviour of Cd^{2+} removal using pyrolysed palm kernel shell (PPKS) as a sustainable biochar adsorbent. Comprehensive material characterization was conducted using Fourier transform infrared spectroscopy (FTIR), scanning electron microscopy coupled with energy-dispersive X-ray spectroscopy (SEM–EDX), thermogravimetric analysis (TGA), Brunauer–Emmett–Teller (BET) surface analysis, and zeta potential measurements to establish structure–property relationships. Batch adsorption experiments were performed to investigate the effects of pH, temperature, contact time, and initial concentration on Cd^{2+} removal efficiency. Kinetic, equilibrium, and thermodynamic analyses were integrated to elucidate adsorption mechanisms and provide a comprehensive understanding of Cd^{2+} removal using biomass-derived carbon materials. The findings contribute to sustainable waste valorisation and offer mechanistic insights for designing low-cost biochar-based adsorbents for practical wastewater treatment applications.

2.0 Materials and Methods

All reagents used in this study were of analytical grade and were used without further purification. Cadmium nitrate [$Cd(NO_3)_2$], phosphoric acid (H_3PO_4; CAS No. 7664-38-2), and sodium hydroxide (NaOH; CAS No. 1310-73-2) were obtained from Merck Chemical Company (Germany).

2.1 Sample Collection

Palm kernel shells (PKSs) were collected from a palm oil processing site located in Ijimo village, Ilesa metropolis, Nigeria. The samples were authenticated at the Department of Crop, Soil and Pest Management, Federal University of Technology, Akure, Nigeria..

2.2 Valorisation of PKSs as Adsorbents and Characterization

The Raw Palm-kernel Shells (RPKSs) were separated from stones and dirt, washed thoroughly with distilled water to remove adhering impurities, dried, and crushed into granules using an industrial grinding machine. The granules were further ground into fine powder using a mortar and pestle. The powder sample was then stored in air-tight containers and labelled for further processing. Approximately 310 g of powdered RPKS was weighed and placed into two clay crucibles. The samples were subjected to pyrolysis in a muffle furnace (Gallenkamp model) at 500 °C under a nitrogen atmosphere for 15 min, sieved through a 106 µm mesh sieve and then stored in sealed plastic containers prior to use. This adsorbent was labelled Pyrolysed Palm-kernel Shell (PPKS) (Barakat *et al.,* 2024; Wipawee & Attso, 2023; Gimba *et al.,* 2001).

A Fourier Transform Infrared (FTIR) spectroscopy (TENSOR 27, Bruker) was used to investigate the adsorbent's functional groups in a wavelength range of 4000 – 500cm^{-1} with a resolution of 8.0 cm^{-1}. Each spectrum was recorded with 200 scans at a scan velocity of 40 kHz. The physical and chemical properties of the prepared biochar were analysed by using several analytical techniques.

The surface morphology and elemental composition of the adsorbents were examined by Scanning Electron Microscopy (SEM, Hitachi SU 3500 scanning microscope, Tokyo, Japan) equipped with Energy Dispersive X-ray (EDX) spectrophotometer. Image scanning and elemental mapping were performed at an accelerating voltage of 30 kV and 12 keV, respectively. The SEM images were taken at 500X magnification. Surface area and pore characteristics were determined using the Brunauer–Emmett–Teller (BET) method through nitrogen adsorption-desorption isotherm at 80 K (ASAP2023 V4.02H, micrometrics, USA). For BET analysis, the samples were degassed at 437 K for 3 h.

The thermal stability of the adsorbents was evaluated using thermogravimetric analysis (TGA). PerkinElmer Thermal Analyzer). In a platinum crucible, 5 mg of each sample, in dried form, was analysed through the analyser under a nitrogen atmosphere of flowing at a rate of 50 mL/min, at a temperature range of 100 – 1000 ºC and heating rate of 10 ºC per minute. The curve for the weight loss was recorded as a function of temperature.

The crystalline phases of the adsorbents were analysed using X-ray diffraction (XRD) spectrometer. The samples to be analysed were oven-dried at a temperature 105 ℃, followed by pulverising to fine powder and sieving to 63 micrometer size. To obtain a flat surface, about 2 g of each sample was mounted on acrylic holder. A Shimadzu XDS 2400H diffractometer with Cu Kα radiation, operating with Cu Kα radiation (λ = 1.5418 Å) at 40 kV and a current of 30 mA was used in collecting patterns of XRD. The diffraction patterns were recorded in a range of 15º – 70º with a step size of 0.02º and a counting time of 2 seconds per step. Search-match comparison with the ICCD Power Diffraction File database was used to carry out phase identification.

An electrokinetic analyser (Surpass 2, Anton Paar, Graz, Australia) was used to determine the zeta potential of the samples. Forty millilitres of buffer solution (with pH 2, 4, 6, 7, 8, 10, and 12) was used in dissolving approximately 8 mg of the adsorbent samples, the solutions formed correspond to a suspension concentration of 0.02% (w/v). The suspensions were mixed properly and allowed to settle for 5 min, followed by the injection of supernatant into the capillary cell of the analyser. Using the Smoluchowski equation zeta potential data were generated through electrophoretic mobility, with measurements in triplicate for 30 s per injection.

2.2 Batch Adsorption Studies, Modelling and Statistical Analysis

A stock solution of cadmium (1000 mg/L) was prepared by dissolving an appropriate mass of $Cd(NO_3)_2$ in distilled water to obtain a 1000 mg L^{-1} Cd^{2+} stock solution. The working concentrations were generated *via* serial dilution. Adsorption experiments were carried out using a batch technique by adding 20 mL of the metal solution to a known mass (e.g. 0.05 g) of prepared adsorbents (RPKS and PPKS) in 50 mL conical flasks. The pH (2, 4, 6, 8, 10) and contact time (2, 5, 10, 15, 20, 30, 60, 240, 480 min) effects on adsorption behaviours were investigated. The pH of the solution was adjusted using 0.5M HCl and 0.5 M NaOH solutions. Initial concentration (50, 100, 150, 200, 300, 400, 500, 600, and 800 mg/L), adsorbent dose (0.01, 0.02, 0.04, 0.06, 0.08, and 1.0 g), and temperature (25, 40, 50, and 60°C) effects were also investigated. The mixtures were agitated at 150 rpm using a thermostatic orbital shaker and filtered to separate the spent adsorbents from unadsorbed adsorbate in the solutions. The final solutions were then analysed for the residual cadmium (II) concentrations after adsorption using an atomic absorption spectrophotometer (AAS; Perkin Elmer Analyst 700 model). Aliquots of the working solutions before adsorption were also analysed to appropriately determine the exact initial concentrations of cadmium (II) ions. The percentage (%) adsorption and the amount of cadmium (II) adsorbed at equilibrium (Q_e) were calculated from the data obtained using equations 1 and 2, respectively.

$$\%Adsorption = \frac{C_o - C_e}{C_o} \cdot 100 \quad (1)$$

$$Q_e = \frac{(C_o - C_e)V}{m} \quad (2)$$

where C_o = initial cadmium(II) concentration (mg/L), C_e= cadmium(II) concentration at equilibrium (mg/L), V = volume of the cadmium(II) solution used for the experiment (L), and m = mass of the adsorbent (g).

The time-dependent adsorption data were subjected to three nonlinear kinetic models (pseudo-first-order, pseudo-second-order, and Avrami fractional) represented by equations 3–5, respectively. The kinetic data were also subjected to the intraparticle diffusion model (equation 6). The concentration and temperature-dependent (isothermal) data were subsequently analysed using non-linear forms of Langmuir, Freundlich, and Liu models shown respectively in equations 7 – 9.

$$Q_t = Q_e\left\{1 - \exp(-k_f t)\right\} \quad (3)$$

$$Q_t = \frac{Q_e^2 k_s t}{k_s Q_e t + 1} \quad (4)$$

$$Q_t = Q_e\left\{1 - \exp(-k_{Av} t)^{n_{Av}}\right\} \quad (5)$$

$$Q_t = k_{id} t^{0.5} + C \quad (6)$$

$$Q_e = \frac{Q_{\max} K_L C_e}{1 + (K_L C_e)} \quad (7)$$

$$Q_e = K_F C_e^{\frac{1}{n_F}} \quad (8)$$

$$Q_e = \frac{q_{\max}(K_g \cdot C_e)^{n_g}}{1 + (K_g \cdot C_e)^{n_g}} \quad (9)$$

From the equations above, Q_t is the amount (mg) of the adsorbate (Cd^{2+}) adsorbed by 1 g of the adsorbents at a particular time, t; k_f (min^{-1}) stands for the rate constant of pseudo-first order; k_s (g mg^{-1} min^{-1}) denotes the rate constant for pseudo-second order; k_{AV} represents Avrami fractional order rate constant (min^{-1}); n_{AV} denotes the Avrami's fractional order, which is related to the mechanism of adsorption; k_{id} is the intraparticle diffusion rate constant (mg g^{-1} $min^{-0.5}$); C (mg g^{-1}) is the intraparticle diffusion constant, which is related to the thickness of the boundary layer; Q_{max} represents the adsorbent maximum adsorption capacity (mg g^{-1}); C_e is the equilibrium concentration of the adsorbent (mg L^{-1}); K_L represents Langmuir equilibrium constant (L mg^{-1}); K_F denotes Freundlich equilibrium constant $\left((mg\ g^{-1})(mg\ L^{-1})^{-\frac{1}{n_F}}\right)$;

n_F is the Freundlich exponent; K_g denotes the equilibrium constant for the Liu model (L mg^{-1}); and n_g is the adsorption intensity (dimensionless).

Thermodynamic equations (equations 10 and 11) were used to calculate the values of the standard change in Gibb's free energy ($\Delta G°$, kJ mol^{-1}), standard change in enthalpy ($\Delta H°$, kJ mol^{-1}) and standard change in entropy ($\Delta S°$, J $mol^{-1}K^{-1}$).

$$\Delta G^o = -RT\ln K \quad (10)$$

$$\ln K = \frac{\Delta S^o}{R} - \frac{\Delta H^o}{RT} \quad (11)$$

where R is the universal gas constant (8.314 J mol^{-1} K^{-1}), T is the temperature in Kelvin (K). Non-linear curve fittings and calculations of parameters were performed on OriginPro. The values of R^2_{adj} (adjusted determination coefficient) and χ^2_{red} (reduced chi square) of each model were used to determine the best model of the adsorption data. The statistical expressions of R^2_{adj} and χ^2_{red} are represented in the equation 12 and 13**,** respectively.

$$R^2_{adj} = \left\{1-(1-R^2)\right\}\left\{\frac{n-1}{n-p-1}\right\} \quad (12)$$

$$\chi^2_{red} = \left\{\frac{1}{n-p}\right\}\sum_i^n \left(q_{i,\exp} - q_{i,model}\right)^2 \quad (13)$$

where n is the number of data points; p is the number of parameters in the model, $q_{i,model}$ and $q_{i,exp}$ are the individual data point predicted by model and obtained by experiment, respectively. A value of R^2_{adj} close to one and high low value of χ^2_{red} signify a good curve fit by a model (Aiyesanmi *et al*., 2022).

3.0 Results and Discussion

Raw palm kernel shell (RPKS) and pyrolysed palm kernel shell (PPKS) adsorbents were prepared from palm kernel shell biomass and comprehensively characterised to evaluate their physicochemical properties. Their adsorption performance toward Cd^{2+} removal from simulated aqueous solutions was systematically investigated using batch adsorption experiments..

3.1 Characteristics of the Adsorbents

The surface chemistry of the adsorbents governs the strength and selectivity of interactions with Cd^{2+} ions, while improvements in textural properties enhance mass transfer during adsorption. Across the adsorbents, FTIR spectra (Fig. 1) show dominant oxygenated functional groups. The thermochemical conversion of Raw Palm Kernel Shell (RPKS) to the broad hydroxyl absorption band at 3400 cm^{-1}, indicates that there were intense dehydration and the loss of cellulosic O–H groups (Biliani *et al.,* 2022). This deoxygenation is further corroborated by the near-total elimination of aliphatic C-H stretching peaks 2850 – 3000 cm^{-1}, which quantifies the demethanation and thermal cleavage of lignin side chains into a more stable, aromatic carbon matrix (Chenyang *et al.,* 2022). As the region of fingerprint moves towards more defined bands near 1000 cm^{-1} to 1200 cm^{-1} vibrations from carbonyl single-bond (C–O) and siloxane (Si–O–Si), the resulting PPKS exhibits a reduced oxygen-carbon (O/C) ratio and elevated hydrophobicity, features that indicate increased carbonisation and improved suitability of the material as an efficient biochar adsorbent. (Rukayat *et al.,* 2024). Contemporary studies highlight that the residual sharp peak near 2300 cm^{-1}, often linked to adsorbed CO_2 or triple-bonded quenching artifacts, may be associated with adsorbed CO_2 species or instrumental artefacts commonly reported in biochar FTIR spectra. (Kwon *et al.,* 2025).

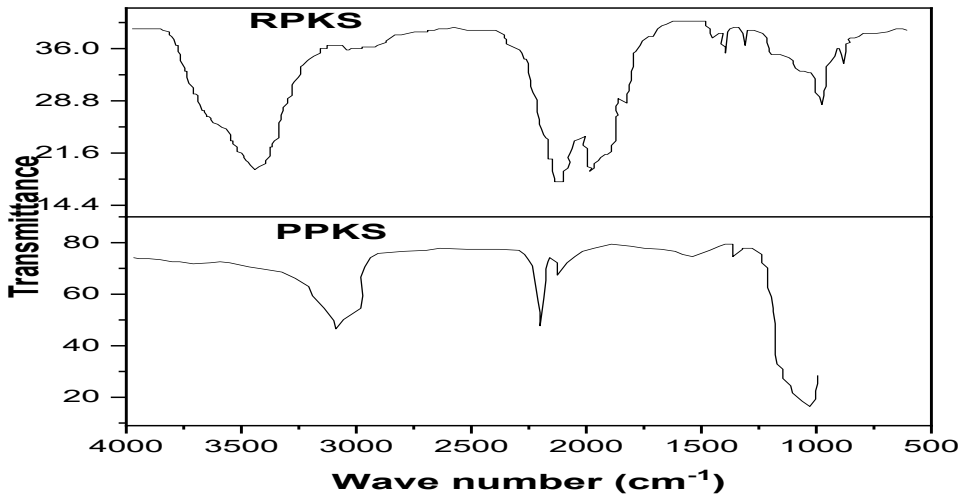

Fig. 1: FTIR spectra of the RPKS and PPKS

Improved thermal stability in activated carbons relative to raw biomass is shown through TGA (Fig. 2). The substantial weight loss observed in RPKS corresponds to moisture evaporation (29.96%) between 150–450 °C and decomposition of hemicellulosic and cellulosic components (51.45%) between 450–570 °C. At temperatures greater than 600 °C, however, PPKS shows higher residual weights (34.01%), indicating an improved condensation of aromatic structure and increased stable carbon content.

These results indicate the formation of a more condensed and thermally stable carbon framework following pyrolysis. As a result of high content of cellulose, a high amount of volatile materials are released when palm-kernel biomass decomposes (Ewa *et al.*, 2024). Similarly, there is a production of low carbon mass in raw palm-kernel biomass when heated (Dechapanya & Khamwichit, 2023). Thermally stable biochars exhibit improved durability, reusability, and retention of surface functionality during repeated adsorption–desorption cycles, an important criterion for real-world water purification systems (Shubhani and Mansoor, 2023).

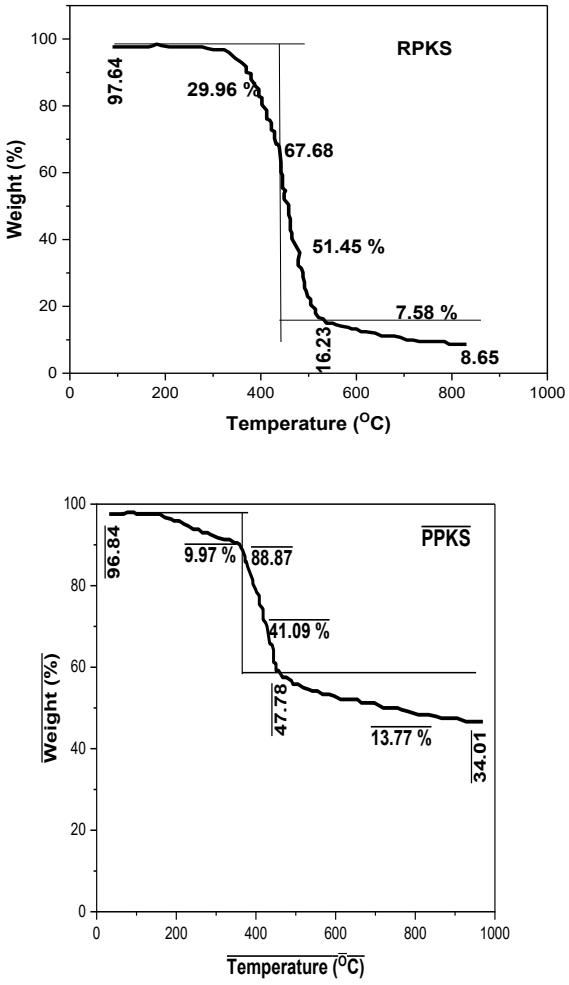

Fig. 2: TGA profiles of RPKS and PPKS

The improved aromaticity and condensed carbon domains in PPKS facilitate prolonged functional lifespan and potentially improved regeneration efficiency when compared to biochars that are not activated.

Morphological analysis (Figure 3) shows a clear and continuous structural transformation from raw palm kernel shell (RPKS) to pyrolysed palm kernel shell (PPKS), highlighting the decisive role of thermochemical modification in tailoring adsorption-relevant properties. Raw palm-kernel shell (RPKS) exhibits a dense, compact, and relatively smooth surface with limited visible pores, characteristic of the native lignocellulosic structure. The retained fibrous framework implies minimal internal surface availability and hindered diffusion routes conditions commonly linked with low particular surface area and poor adsorption efficiency. Dadhich *et al.* (2025) noted that comparable morphological features have been indicated for untreated agricultural wastes, where the structural quality of cellulose-hemicellulose-lignin matrices limits pore formation and reduces the removal of metal ion primarily to functional groups at the surface.

PPKS shows a significant rearrangement of the structural framework through physical pyrolysis. The surface appears significantly rougher, with the appearance of irregular cavities, fissures, and partially developed pore structures. These transformations are ascribed to devolatilization and thermal breakdown of cellulose and hemicellulose, associated with continuous aromatisation and carbon framework rearrangement during carbonization. Such attributes are aligned with conventional pyrolysis mechanisms for lignocellulosic starting materials that easily improve adsorption performance *via* elevated surface area and improved accessibility of active sites (Fanzhi *et al*., 2022). Conversely, PPKS indicates pore structure which appears partially collapsed and irregular in some regions, indicating that physical activation alone may not fully enhance development of hierarchical pore, as opening of structural networks and tar accumulation can reduce connectivity of pore (Anastasia *et al*., 2022).

The SEM image of PPKS indicates enlarged pores, distinct cavity walls, and a more homogeneous pore distribution compared to RPKS. This morphology is attribute of phosphoric acid activated the sample, in which dehydration reactions, bond breaking, cross-linking, and matrix swelling during thermal treatment produce widespread micro- and meso-porosity. The resulting hierarchical structure through the combination of micropores and mesopores for both higher specific surface area and swift mass transfer is broadly established as optimal for heavy metal adsorption, as it decreases the resistance of intraparticle diffusion and enhances kinetics of adsorption (He *et al.,* 2025). The increase in pore volume and surface area directly contributes to enhanced adsorption capacity by increasing the number of accessible active sites. The observed structural evolution confirms that pyrolysis enhances pore development and increases accessible adsorption sites responsible for improved Cd^{2+} uptake.

Quantitative EDX (Fig. 4) analysis shows that PPKS has elevated carbon (63.03%) more than the RPKS carbon content (57.85%). There is corresponding increase in oxygen levels, with RPKS = 15.73% and PPKS = 26.97%, indicating elemental redistribution resulting from thermal and chemical activation processes. In addition, higher calcium was noted from 9.64% in RPKS to 12.64% in PPKS, with potassium reduced significantly from 4.61% to 2.60% in PPKS while RPKS showing 2.48%, suggesting mineral transformation and partial volatilisation during pyrolysis. Small quantities of other minerals such as Mg = 0.65 – 0.88%, Na = 0.93%, Si = 0.14 – 0.82%, P = 0.02 – 0.07%, and Fe

=1.32% remained at trace-to-low concentrations from PPKS to RPKS, but promote cation-exchange functionality and surface heterogeneity.

Hongyan *et al.* (2022) noted that reduction in oxygen-carbon ratios, and controlled mineral conversion improve biochars surface stability, aromaticity, and divalent metal adsorption efficiency, and these are consistent with the result of the current study from the significant decrease in oxygen content from RPKS to PPKS, and increase in carbon conten

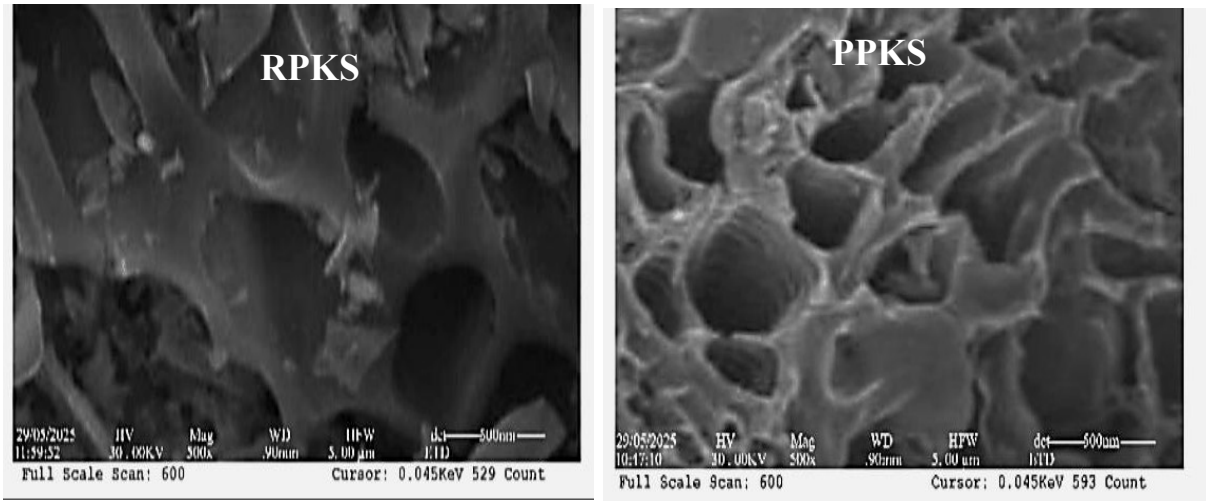

Fig. 3: Scanning electron micrographs of RPKS and PPKS

t.

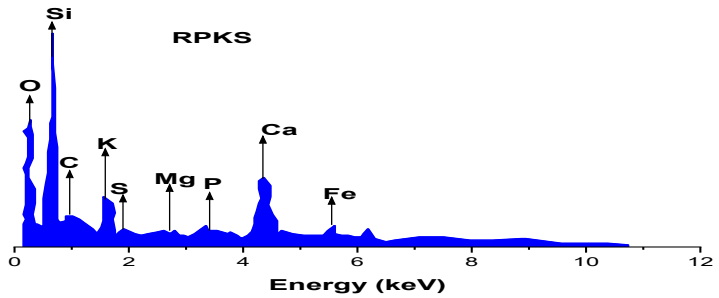

Elements (RPKS)	Percentage (%)
C	57.85
O	15.73
Ca	9.64
P	0.07
Si	0.14
K	2.48
Na	0.93
Mg	0.65
S	0.22

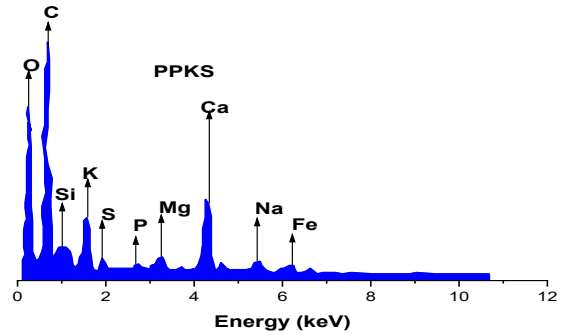

Elements (PPKS)	Percentage (%)
C	63.03
O	26.97
Ca	12.64
P	0.02
Si	0.82
K	4.61
Na	0.93
Mg	0.88
S	0.01

Fig. 4: EDX spectra (and elemental compositions) of RPKS and PPKS

eta potential (Fig. 5) is a pivotal parameter foZr determining the surface charge properties of adsorbents and thus their interaction mechanisms with ionic contaminants in aqueous media.

The point of zero charge (PZC) represents the pH at which the net surface charge of the adsorbent becomes electrically neutral (Nuhu *et al*., 2025). The results presented indicate that the *PZC* of RPKS and PPKS are 5.80, and 5.73, respectively. The adsorption of anions (negative charge particles) increases when the surfaces of the adsorbents become highly positive charge due to the decrease in their respective pH of their solutions below the point of zero charge values while the adsorption of cations (positive charge particles) increases when the pH values of their solutions are more than their respective values of their point of zero charge (*PZC*). The highest *PZC* is obtained in the raw palm-kernel chaff (RPKS), indicating a reduced level of some acidic functional groups, including phenolic, lactonic moieties, and carboxyl groups, which can easily reduce the electrical charge neutrality at the surface of the adsorbents (Sobik-Szołtysek *et al.,* 2021).

Functional groups such as carboxylic-ester, ether-alcohol, and aliphatic groups have increased the negative charge on the surface of microplastic particles at pH of solution greater than 2.0 which continuously increased the density of acid site **(**Jui-Yen *et al.,* 2023). The reduced *PZC* value obtained in the PPKS may be linked to the presence of the mineral oxides in the adsorbent. These hetero-atoms can easily affect the arrangements of electrons, thereby changing the surface charge property by enhancing the acidity of the surface and in turn, reducing the *PZC* (Pan *et al.*, 2022).

XRD trends (Fig. 6) reveal substantial variations in the carbon structural order across sample materials. RPKS indicates clear crystalline peaks linked with inherent lignin and cellulose **(**Khandoker *et al.,* 2023). Conversely, PPKS displayed broad diffuse peaks around 2θ (20^{O} to 60^{O}) characteristic of amorphous carbon structures with turbostratic ordering formed during carbonization The loss of crystalline cellulose peaks validates thermal breakdown and carbonisation during pyrolysis and activation mechanisms. Amorphous carbon frameworks exhibit high level of active sites and structural defects that are beneficial for heavy metal adsorption owing to unsaturated coordination environments (Kun *et al.,* 2024). The increase in structural disorder enhances the density of active adsorption sites and defect regions favourable for metal ion binding.

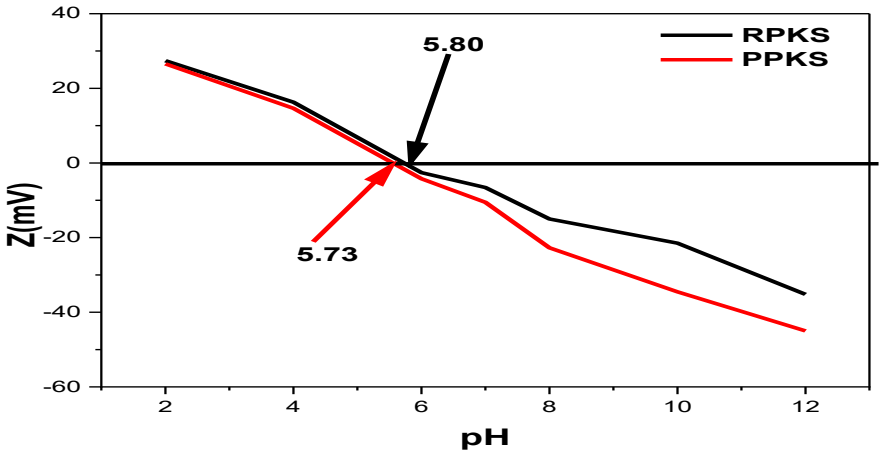

Fig. 5: Zeta potentials of RPKS and PPKS

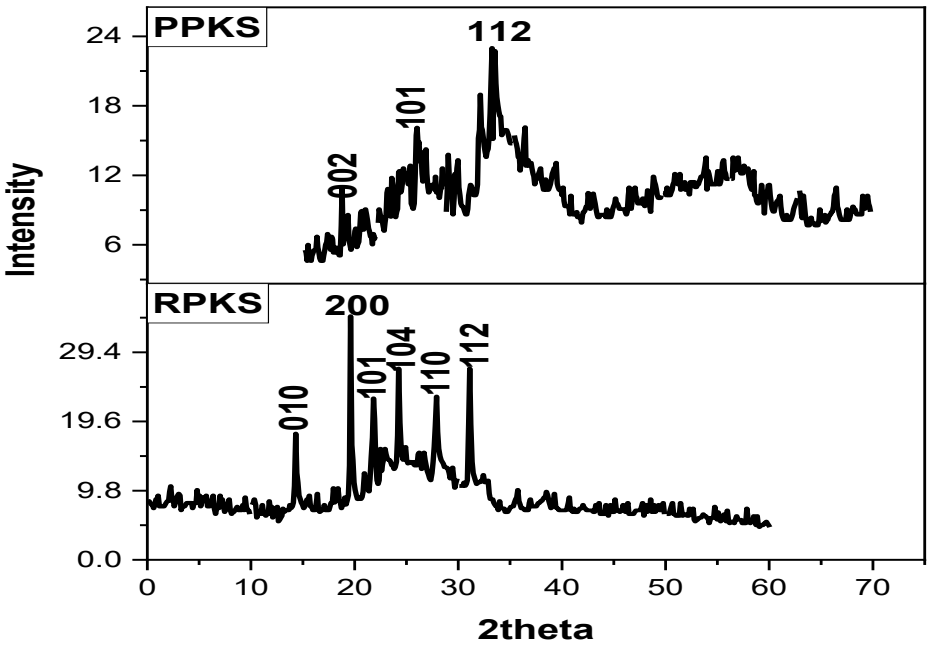

Fig. 6: X-ray diffraction (XRD) of the adsorbents

Such sites can interact with Cd^{2+} through π–cation interactions or *via* coordination with heteroatoms, improving adsorption which exceeds simple electrostatics process. Contemporary Studies in carbon has highlighted the influence of disordered carbon structures in promoting elevated concentrations of adsorption reactive sites for metal and organic pollutant, specifically in chemically activated biochars (Benhadj *et al.,* 2026).

Brunauer–Emmett–Teller (BET) nitrogen adsorption–desorption analysis results are presented in Table 1. Specifically, PPKS exhibits the high surface area (112.905 m^2/g), pore diameter (2.2023 nm) and total pore volume (1.0086 cm^3/g), strongly suggesting a more developed porous network that provides a greater number and accessibility of adsorption sites for Cd^{2+} ions compared with RPKS. This observation is consistent with current reviews showing that an increased internal and external surface area elevated adsorption of ions onto the active sites, also high pore volumes promote diffusion of metal ions and mass transport into the inner pore structure of carbonaceous adsorbents, resulting in higher capacities of adsorption in aqueous remediation applications (Padmaja *et al.,* 2024; Raji *et al.,* 2023). Increase in the pore volume has resulted in the enlargement and merging of the pores. When micro-pores merge into meso-pores, overall pore volume rises sharply but the specific surface area does not increase proportionally, and in some cases can decrease (Neme *et al.,* 2022).

The present study with approximate pore diameters range 2.2023 to 2.2682 nm are with pores in the mesopore range, which are especially beneficial for heavy metal adsorption because they strike a balance between providing accessible pathways for hydrated Cd^{2+} species and maximizing contact with the internal surface, thereby reducing diffusion resistance and enhancing uptake efficiency (Masud *et al.,* 2021). Moreover, there is a progressive structural development due to the hierarchical increase in BET surface area and pore volume from RPKS to PPKS, and this likely reflecting more efficient activation and formation of pores which results in enhanced performance in the removal of Cd^{2+}

reported in recent adsorbent investigations using activated carbons derived from agricultural waste materials (Padmaja *et al.,* 2024). Studies have shown that consecutive increase in the surface areas at pyrolysis temperature 400 to 600 ℃, as observed in RPKS and PPKS lead to increase in access pores for pollutants to diffuse and get adsorbed (Neme *et al.,* 2022; Zakaria *et al.,* 2023).

Table 1: BET data of RPKS and PPKS

Adsorbent	BET Surface area (m^2/g)	Pore diameter (nm)	Pore volume (cm^3/g)
RPKS	103.750	2.2682	0.5938
PPKS	112.905	2.2023	1.0086

3.2 Adsorption Performances of RPKS and PPKS at varying pH Values

The Cd^{2+} adsorption behaviour (Fig. 7A) exhibits a strong pH-dependent adsorption behaviour, an attribute of advanced biochar systems documented in a recent study (Zhao *et al.,* 2025). Quantitatively, removal efficiencies increased from about 53 to 70% in the acidic region (pH < 4) to peak values of approximately 88 – 96% at pH 5 – 6, with the performance order PPKS (~92%) > RPKS (~89%), before declining to approximately 50 – 70% under alkaline conditions (pH > 7). These results confirm that electrostatic attraction and surface complexation jointly govern Cd^{2+} adsorption.

At low pH, higher concentrations of H^+ ions compete with Cd^{2+} for functional groups containing oxygen atoms (–COOH, –OH), resulting to protonation of the surface of adsorbent and electrostatic repulsion, thereby decreasing the uptake. At pH 5 – 6, continuous deprotonation results in increase negative surface charge density, improving ion-exchange interactions, electrostatic attraction, and inner-sphere complexation, as Cd^{2+} remains predominantly soluble; conditions broadly documented as optimal for Cd^{2+} adsorption onto activated carbons and engineered biochars (Huang and Imran, 2025; Saeed *et al.*, 2021).

The high efficiency of PPKS shows that combination of physical activation majorly improves surface functionality and pore accessibility, complexation affinity, and rising active site density consistent with recent mechanistic studies (Ivan and Iryna, 2025). The reduction noted above neutral pH may show altered Cd speciation such as the formation of $Cd(OH)^+$ and partial precipitation as $Cd(OH)_2$, which decreases the inherent contribution of main adsorption mechanisms. Overall, the quantitative enhancement sequence and optimal pH window align with contemporary adsorption theory, confirming that chemically activated palm-kernel-derived biochars operate within the high-efficiency range reported for carbonaceous adsorbents (Nuñez-Vargas *et al.,* 2026).

The experimental data (Fig. 7B) illustrate a significant positive correlation between adsorbent dosage and the percentage adsorption of Cd^{2+} by RPKS and PPKS. The percentage range (10% to 15%) of adsorption performance occurred at the lowest dosage of 0.01 g. Furthermore, a sharp linear elevation in adsorption was noted as the dosage continues to 0.06 g, where equilibrium position began. Particularly, PPKS demonstrated the highest efficiency, achieving near-quantitative removal of approximate value 94 % and RPKS approximate 75%. As a result of an increase in the mass of adsorbent, Adeleke *et al.* (2023) emphasised a pattern associated with a greater number of active sites for adsorption and a larger surface area that is effective. As the dosage is more than 0.06 g mass there exists plateau pattern on the graphs, indicating that either site aggregation occurred or an equilibrium position is reached where the Cd^{2+} ions were no longer the limiting factor. As

noted by Chukwunoso *et al.* (2021) that this effectively stabilised the removal percentage even as the dosage was increased to 1.0 g.

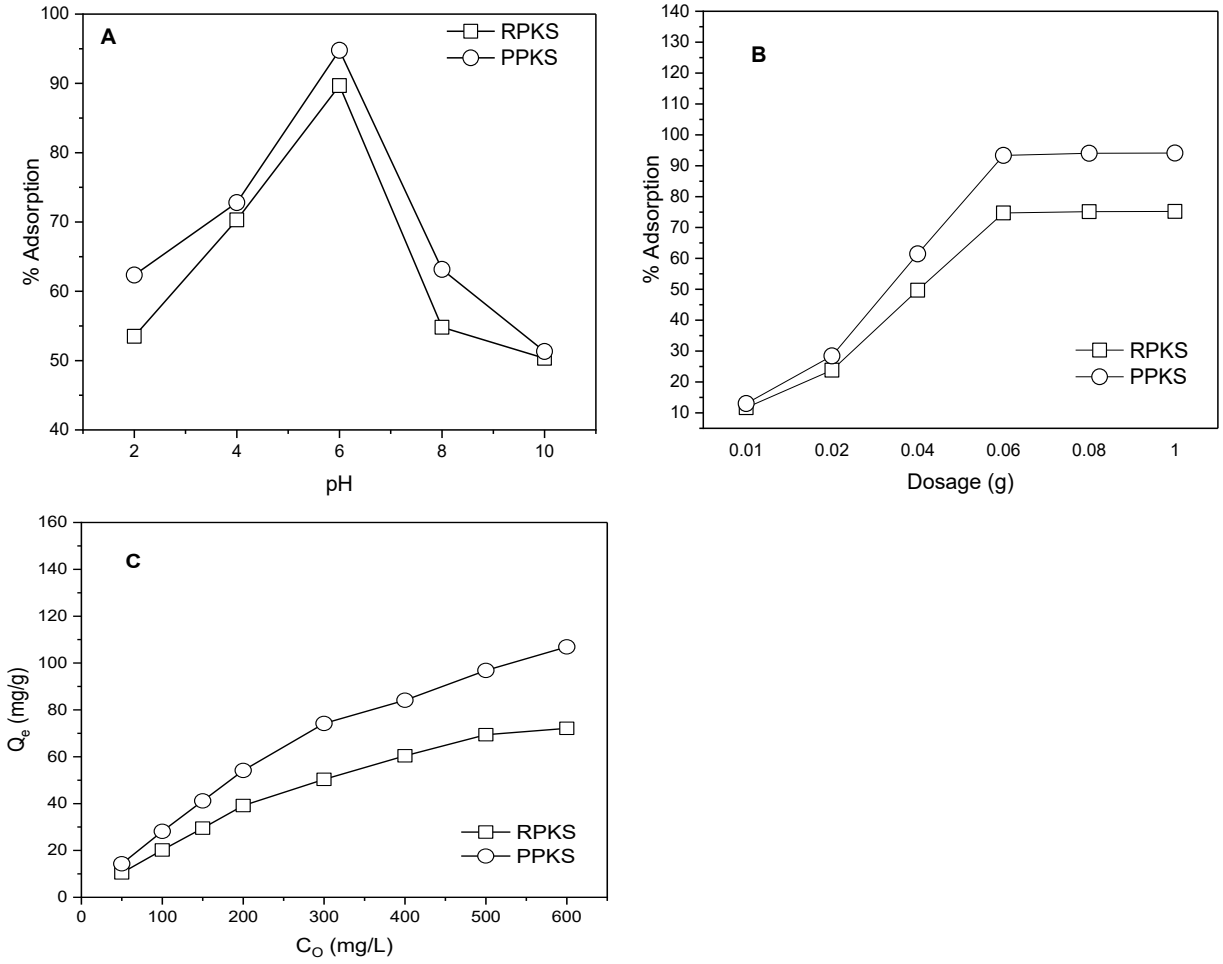

Fig. 7: (A) pH profiles, (B) dosage profiles, and (C) effect of initial [Cd^{2+}] on adsorption of Cd^{2+} onto RPKS and PPKS

The graph (Fig. 7C) clearly explains the relationship between the initial concentration (C_o) of Pb^{2+}ions in solutions and the adsorption capacity at equilibrium (Q_e) for the adsorbents under study. The data observed in the adsorption show a significant improvement in the removal of cadmium(II) (Cd^{2+}) ions after palm-kernel shell (PKS) has been subjected to thermal process. The amount of the metal adsorbed by RPKS increased from 10.5 to 72.1 mg/g as initial concentration (C_o) increased from 50 mg/L to 600 mg/L, while 107.4 mg/g is obtained in pyrolysed Palm-Kernel shell (PPKS), showing about 49% enhancement. This superior performance is consistent with recent findings that pyrolysis/carbonisation of lignocellulosic biomass significantly improves specific surface area, pore development, and the availability of oxygenated functional groups, thereby strengthening Cd^{2+} complexation and electrostatic interactions (Obey *et al.,* 2024).

PPKS retains high capacity at increased amounts of the adsorbate due to enhanced accessibility of the pore accessibility and surface reactivity, emphasizing its greater

suitability for the removal of large amounts of cadmium(II) from aquatic environments while in RPKS quick surface saturation of active sites is observed, and represented by the plateau on the graph. As shown in the figure, as the value of equilibrium adsorption capacity (Q_e) increases steadily as the initial concentration of cadmium(II) ions increases. This phenomenon indicates that for a unit mass of adsorbent, an increase amount of Pb^{2+} ions is being adsorbed and this may be due to the available active sites on the adsorbent's surface. Increasing initial Cd^{2+} concentration enhances the concentration gradient, thereby increasing the mass-transfer driving force and adsorption capacity. High ion diffusion and site utilisation occur until surface sites are completely occupied as a result of an increase in initial concentration of heavy metal solution (C_0) and that of equilibrium adsorption capacity (Q_e) (Yan *et al.,* 2023).

3.3 Kinetic Modelling of the Adsorption Process

The kinetic graphs (Fig. 8) show a fast initial cadmium(II) (Cd^{2+}) adsorption onto RPKS and PPKS owing to its strong electrostatic interactions and availability of active sites, with a progressive attainment of equilibrium as the driving force reduces the surface saturation. The intraparticle diffusion plots exhibit multilinearity with non-zero intercepts, indicating that while pore diffusion contributes to Cd^{2+} uptake, it is not the sole rate-limiting step; instead, the overall mechanism is governed by a combination of film diffusion and intraparticle transport.

Estimation of the kinetic parameters of Cd^{2+} adsorption onto RPKS and PPKS provided substantial findings into the adsorption mechanisms, surface properties, and energetic requirements of these adsorbents through the use of different kinetic models such as pseudo-first order, pseudo-second order, Avrami, and intraparticle diffusion. These models were applied on the kinetic data to obtain the rate constants, the order of adsorption process, and to predict the model that best described the experimental kinetic data. The kinetic profiles and parameters are represented in the Fig. 8 and Table 2, respectively.

The kinetic modelling for the adsorption of Cd^{2+} onto RPKS and PPKS reveals a complex mechanism where surface heterogeneity and chemisorption interact. Model suitability was evaluated using the correlation coefficient (R^2) and error function values represented by R^2_{adj} and χ^2_{red}. The best fitting model is regarded as the model with the highest value of R^2_{adj} and the lowest value of χ^2_{red}. The data supplied in Table 2 show that Avrami fractional order kinetic model provided the best fit with highest R^2_{adj} and lowest χ^2_{red}. The values of k_{AV} (Avrami fractional order rate constant) are 0.095260 and 0.075030 min^{-1} for RPKS and PPKS, respectively; these values signified that sorption onto RPKS occurred at a slightly faster initial rate than PPKS, although PPKS exhibited higher overall adsorption capacity. The exponents (n_{AV}) of approximately 0.56, which indicates that a non-integer kinetic pathway likely involving multiple mechanisms or a change in the adsorption rate as surface coverage increases **(**Xinlei *et al.*, 2025**)**.

3.4 Equilibrium Description of the Adsorption Process

The equilibrium adsorption behaviour is used to describe the distribution of adsorbate molecules between the liquid phase and adsorbent surface at equilibrium. Langmuir, Freundlich, and Liu equilibrium models were used to elucidate the adsorption behaviour of Cd^{2+} ions onto the RPKS and PPKS adsorbents at different temperatures (25 °C – 60 °C).

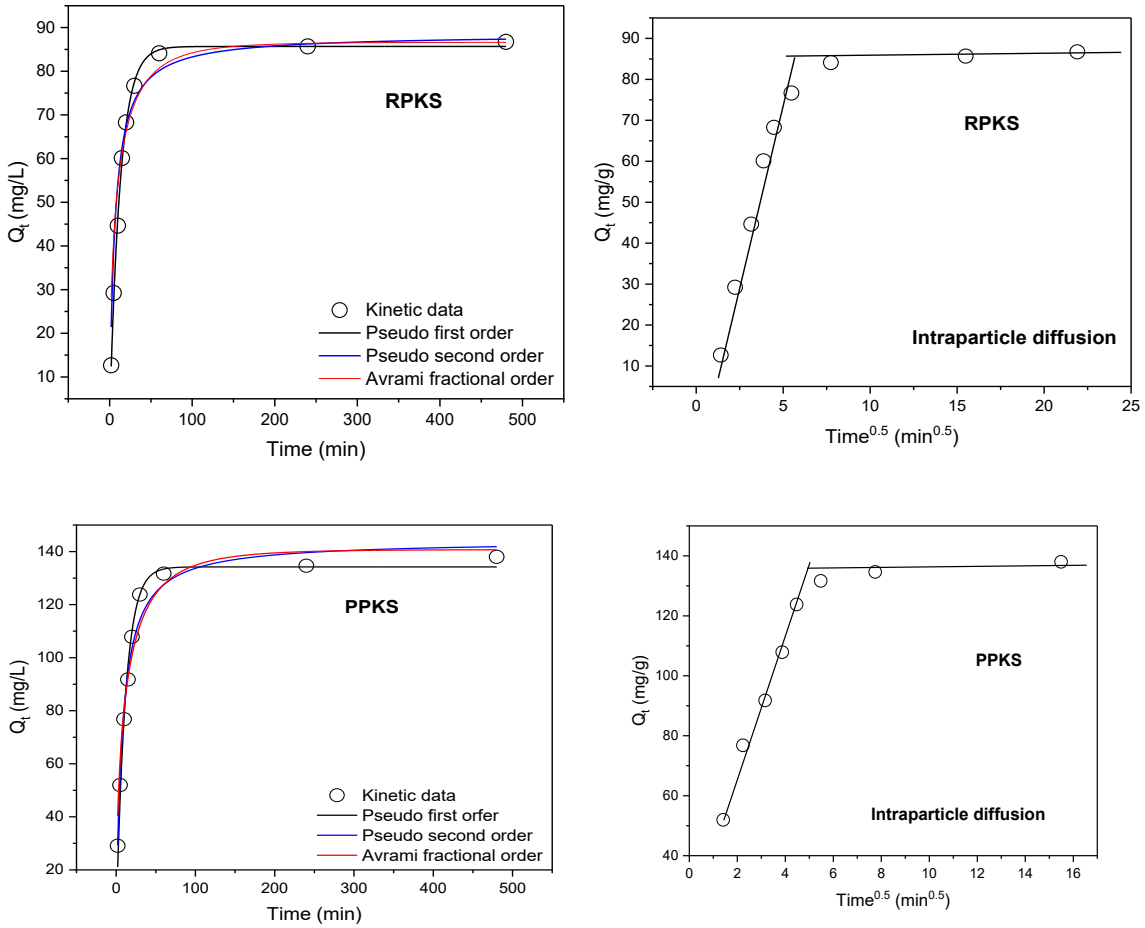

Fig. 8: Kinetic profiles of RPKS and PPKS for adsorption of Pb^{2+}
Conditions: pH = 6; Dosage = 0.06 g; Agitation time: 2 – 480 min; Temperature = 25 °C

Table 2: Kinetic parameters for adsorption of Cd^{2+} onto RPKS and PPKS

Model	Parameters	Values	
		RPKS	PPKS
Pseudo-first order	$Q_{e,exp}$ (mg/g)	84.097	131.67
	$Q_{e,cal}$ (mg/g)	85.665	134.21
	k_f (min^{-1})	0.078340	0.085440
	R^2_{adj}	0.98837	0.988460
	χ^2_{red} (mg/g)	1.3326	20.113
Pseudo-second order	$Q_{e,cal}$(mg/g)	88.486	144.17
	k_s (g/mg min)	0.0018000	8.8421×10^{-4}
	R^2_{adj}	0.91476	0.98302
	χ^2_{red} (mg/g)	6.4622	29.586
Avrami fractional order	$Q_{e,cal}$ (mg/g)	86.631	140.74
	k_{AV} (min^{-1})	0.095260	0.075030

	n_{AV}	0.56527	0.57295
	R^2_{adj}	0.99361	0.99271
	χ^2_{red} (mg/g)	0.56265	1.4499
Intraparticle diffusion	k_{id} (mg/g min$^{0.5}$)	16.284	22.477
	R^2_{adj}	0.97884	0.99089
	C (mg/g)	–7.4110	42.266

The isotherm curves and data parameters are presented in respective Fig. 9 and Table 3.

The data in the table showed that Liu model is the best fit model for adsorptoion of cadmium(II) onto the two adsorbents. Study shows that one of the significant assumptions of Liu model is that the active sites on the adsorbent surface possess varying values of energy (Naifar *et al.,* 2025). In this present study, the Liu maximum adsorption capacities (Q_{max}) for RPKS (5748.4 mg/g at 25 °C, 78.180 mg/g at 40 C, 2387.7 mg/g at 50 °C, and 1259.3 at mg/g at 60 °C) while PPKS (3090.9 mg/g at 25 °C, 5069.2 mg/g at 40 °C, 4914.2 mg/g at 50 °C and 97.104 mg/g at 60 °C. Adsorbent PPKS has the high adsorption capacity for the removal of aqueous Cadmium(II) ions and the better performance of PPKS than RPKS can be linked to effect of pyrolysis.

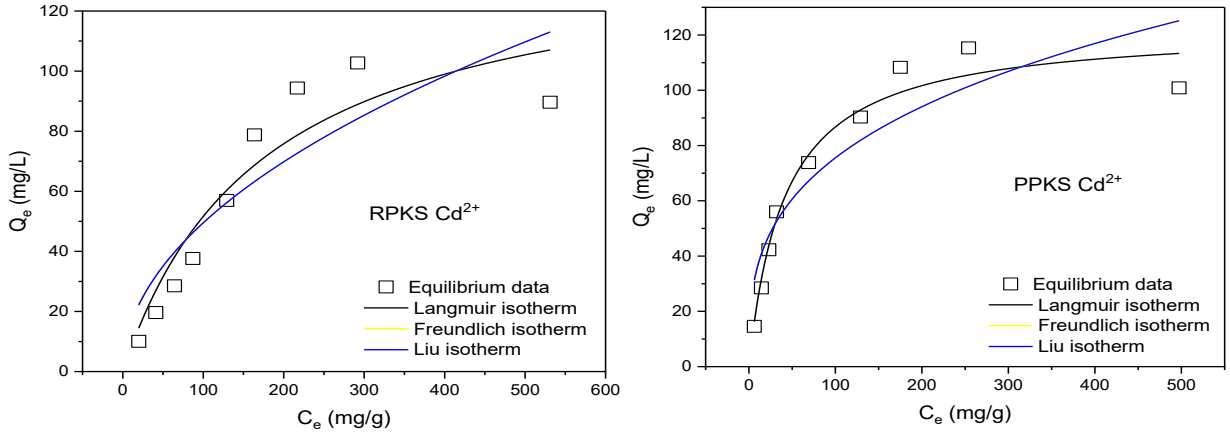

Fig. 9: Equilibrium profiles for the adsorption of Cadmium(II) onto RPKS and PPKS Conditions: pH = 6; dosage = 0.06 g; agitation time = 2 h; Temperature = 25°C; [Pb^{2+}] = 50 – 500 mg/L

Table 3: Equilibrium parameters for the adsorption of Cd^{2+} onto RPKS and PPKS

Model	**Parameters**	**Values**			
RPKS		**25 °C**	**40 °C**	**50 °C**	**60 °C**
Langmuir	Q_{max} (mg/g)	142.52	104.42	69.238	46.607
	K_L (L/mg)	0.32884	0.53677	0.68922	0.86746
	R^2_{adj}	0.88690	0.901442	0.91420	0.90109
	χ^2_{red} (mg/g)	158.39	73.174	29.949	14.786
Freundlich	$K_F\left((mg\ g^{-1})(mg\ L^{-1})^{-\frac{1}{n_F}}\right)$	5.0762	3.6382	3.7400	2.7876
	n_F	2.0218	2.0447	2.3459	2.4845

	R^2_{adj}	0.78467	0.80917	0.80807	0.97058
	χ^2_{red} (mg/g)	301.56	141.68	66.997	4.6902
Liu	Q_{max} (mg/g)	5748.4	78.180	2387.7	1259.3
	K_g (L/mg)	0.32884	0.53677	0.68922	0.86746
	n_g	0.50109	0.86140	0.43367	0.41106
	R^2_{adj}	0.99999	0.94385	0.99999	0.99999
	χ^2_{red} (mg/g)	0.0020552	48.640	6.9880	1.8516
PPKS					
Langmuir	Q_{max} (mg/g)	122.80	137.77	121..52	97.104
	K_L (L/mg)	0.12466	0.31280	0.48569	0.75413
	R^2_{adj}	0.96519	0.92069	0.92286	0.89121
	χ^2_{red} (mg/g)	53.011	119.91	79.640	70.278
Freundlich	$K_F\left((mg\ g^{-1})(mg\ L^{-1})^{-\frac{1}{n_F}}\right)$	17.641	8.9766	4.9435	3.4155
	n_F	3.1674	2.3825	2.1052	2.0560
	R^2_{adj}	0.83810	0.80689	0.83418	0.80642
	χ^2_{red} (mg/g)	246.55	291.96	171.20	125.05
Liu	Q_{max} (mg/g)	3090.9	5069.2	4914.2	3856.3
	K_g (L/mg)	0.12466	0.31280	0.48569	0.75413
	n_g	0.32507	0.42668	0.48147	0.49296
	R^2_{adj}	0.99999	0.99999	0.99999	0.99999
	χ^2_{red} (mg/g)	0.0067535	0.0031225	0.0016414	9.8367 x 10^{-4}

3.5 Thermodynamic Characteristics of the Adsorption Process

Adsorption behaviour of the palm-kernel shell at different values of temperature was predicted *via* investigation of thermodynamic parameters. The range of temperature used in this present investigation has a considerable effect on adsorption process. The thermodynamic data for standard enthalpy change ($\Delta H°$), standard entropy change ($\Delta S°$), standard Gibb's free energy ($\Delta G°$), and the linear van't Hoff's graphs of $ln\ K_g$ against T^{-1} for the two adsorbents are represented in the Table 4 and Fig. 10. The thermodynamic data were modelled to demonstrate the effect of temperature on the adsorption process. The standard Gibb's free energy ($\Delta G°$) values ranged from –8.9440 to –12.680 kJ/mol for RPKS (298 –333 K), and from –6.5408 to –12.292 kJ/mol for PPKS (298 – 333 K), respectively. The spontaneity and feasibility of the process is confirmed by the negative values of $\Delta G°$.

The values of standard change in enthalpy ($\Delta H°$) and standard entropy change ($\Delta S°$) were calculated from the respective slopes and intercepts of van't Hoff's graphs. The adsorption process was endothermic (positive values of $\Delta H°$) (Ahsan *et al.,* 2018) while the positive values of $\Delta S°$ of the adsorbents under study for Cd^{2+} uptake exhibited an increase in the randomness at the interface of solid-liquid interaction. Study showed that mechanism of

adsorption can be determined by standard entropy change, in that for $\Delta S° > 10$ J/mol K indicate dissociative mechanism while $\Delta S° < 10$ J/mol K indicating associative mechanism (Abbasizadeh *et al.,* 2014; Shafiee *et al.,* 2020). The dominant mechanism in this present study is dissociative because the values of $\Delta S°$ obtained are greater than 10 J/mol K for Cd^{2+} adsorption.

Table 4: Thermodynamic parameters for Cd^{2+} for RPKS and PPKS

Adsorbent	Temperature (K)	K_g (L/mg)	K_g (m^3/mol)	ΔG^o (kJ/mol)	ΔS^o (J/mol K)	ΔH^o (kJ/mol)	R^2_{adj}
RPKS	298	0.32884	36.966	–8.9440	98.844	20.2384	0.99981
	313	0.53677	60.340	–10.669			
	323	0.68922	77.478	–11.682			
	333	0.86746	97.514	–12.680			
PPKS	298	0.12466	14.013	–6.5408	149.29	37.437	0.99985
	313	0.31280	35.163	–9.2641			
	323	0.48569	54.598	–10.742			
	333	0.75413	84.775	–12.292			

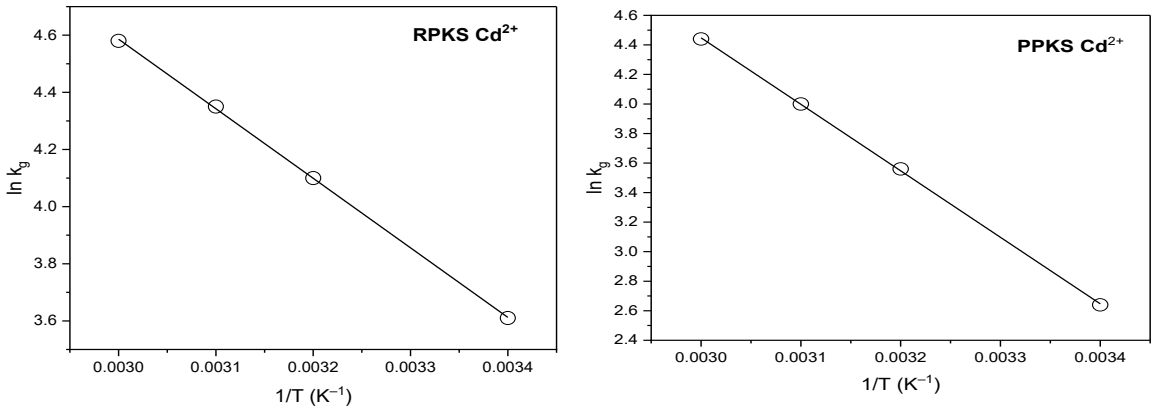

Fig. 10: vant-Hoff plots for adsorption of Cd^{2+} onto RPKS and PPKS

4.0 Conclusion

The present study reveals the structural framework, adsorption performance, and mechanistic routes controlling adsorption of cadmium(ii) (Cd^{2+}) ions onto raw and pyrolysed palm kernel shell (PPKS). Thermochemical transformation markedly improved functional groups at the surface, carbon content, mesoporosity (112.91 m^2/g), and thermal stability of PPKC when compared with RPKS, corroborating viable physicochemical conversion. Zeta potential assessment and FTIR data demonstrated the key function of surface deprotonation and oxygenated functional groups in facilitating electrostatic attraction and surface complexation at maximum pH 5 – 6, where more than 90% removal efficiencies occurred. Kinetic modelling showed that the Avrami fractional order model best explained the process of adsorption than the pseudo first order and pseudo second order, implying multiple step mechanisms which involve mass transfer at the surface and heterogeneous surface bindings. Equilibrium data were most

closely fitted by the Liu isotherm, underscoring energetic heterogeneity and combination of Langmuir and Freundlich behaviour. Thermodynamic parameters with $\Delta G° < 0$; $\Delta H° > 0$, validated spontaneous and endothermic adsorption. Collectively, pyrolysed palm kernel shell establishes elevated performance of adsorption process, mechanistic reliability, and structural resilience, designating palm kernel shell as an eco-friendly, cost-effective, and adsorbent that aligned with the circular economy goals for the remediation of cadmium in environmental wastewater.

5.0 References

Awaka-Ama, J. J., Udo, G. J., Uwanta, E. J., Etukudo, N. J., Akpanudo, N. W., & Igwe, R. (2024). Comparative analysis of heavy metal contamination in regular and artisanal petroleum products in Akwa Ibom State, South-South Nigeria. *Communication in Physical Sciences*, 11, 3, pp. 559–568.

Ladan, M., Muhammad, K. Z., & Habibu, S. (2026). Enhanced adsorptive removal of Pb^{2+} and Cd^{2+} ions from aqueous solution using phosphoric acid–activated rice husk. *Journal Name*, 13, 2, pp. 307–328.

Akpanudo, N. W., & Chibuzo, O. U. (2020). Musanga cecropioides sawdust as an adsorbent for the removal of methylene blue from aqueous solution. *Communication in Physical Sciences*, 5, 3, pp. 362–370.

Nuhu, J. S., Awe, F. E., Garg, R., Garg, R., Eddy, N. O., & Paktin, H. (2025). Cobalt titanate nanocatalyst for enhanced photodegradation of atrazine: Kinetics, degradation efficiency, and mechanistic analysis. *BMC Chemistry*, 19, 31, pp. 1–12. https://doi.org/10.1186/s13065-025-01394-5

Abbasizadeh, S., Keshtkar, A. R., & Mousavian, M. A. (2014). Sorption of heavy metal ions from aqueous solution by a novel cast PVA/TiO_2 nanohybrid adsorbent functionalized with amine groups. *Journal of Industrial and Engineering Chemistry*, 20, 4, pp. 1656–1664.

Adeleke, A. E., Onifade, A. P., Sangoremi, A. A., Anifowose, A. J., Isola, O. E., & Olawoye, B. M. (2023). Adsorption of Pb^{2+}, Co^{2+}, and Cd^{2+} from aqueous solution using nitric acid modified kola nut husk adsorbent. *Journal of Applied Sciences and Environmental Management*, 27, 5, pp. 919–925. https://doi.org/10.4314/jasem.v27i5.5

Ahsan, M. A., Islam, T., Hernandez, C., Castro, E., Katla, S. K., Kim, H., Lin, Y., Curry, M. L., Gardea-Torresdey, J., & Noveron, J. C. (2018). Biomass conversion of saw dust to a functionalized carbonaceous material for the removal of tetracycline, sulfamethoxazole and bisphenol A from water. *Journal of Environmental Chemical Engineering*, 6, 4, pp. 4329–4338.

Barakat, N. A. M., Mahmoud, M. S., & Moustafa, H. M. (2024). Comparing specific capacitance in rice husk-derived activated carbon through phosphoric acid and potassium hydroxide activation order variations. *Scientific Reports*, 14, 1460, pp. 1–12. https://doi.org/10.1038/s41598-023-49675-0

Benhadj, M., Alouiz, I., Amarouch, M. Y., Sennoune, M., & Mazouzi, D. (2026). From lignocellulosic biomass to activated carbon: Impact of composition, structure and activation on the adsorption of organic pollutants. *Scientific African*, 31, e03249, pp. 1–15. https://doi.org/10.1016/j.sciaf.2026.e03249

Biliani, S. E., Vakros, J., & Manariotis, I. D. (2022). Screening of raw and modified biochars from food processing wastes for the removal of phosphates, nitrates, and ammonia from water. *Sustainability*, 14,

24, pp. 16483–16498. https://doi.org/10.3390/su142416483

Centelles, J. J., Moreno, E., de Atauri, P. R., & Imperial, S. (2024). Problem-based learning for calculating kinetic parameters from Michaelis-Menten equation. *International Journal on Engineering, Science, and Technology*, 6, 1, pp. 55–67. https://doi.org/10.46328/ ijonest.161

Chenyang, W., Shengpeng, X., Chaoxian, C., Shunshun, K., Anqing, Z., Zhaosheng, Y., & Zengli, Z. (2022). Investigation into the correlation between the chemical structure of lignin and its temperature-dependent pyrolytic product evolution. *Fuel*, 329, 125215, pp. 1–10. https://doi.org/10.1016/j.fuel.2022.125215

Chukwunonso, O. A., Elshkankery, M., Fletcher, A. J., Osama, M. M., Abdel-Halim, E. S., & Hashem, A. (2021). Equilibrium and kinetic modelling of aqueous cadmium ion and activated carbon adsorption system. *Water Conservation Science and Engineering*, 6, 2, pp. 1–12. https://doi.org/10.1007/s41101-021-00107-y

Dadhich, A., Dhar, I., Choudhary, R., Sharma, Y., Sharma, M. M., & Jain, R. (2025). Lignin-driven valorization of lignocellulosic biomass to functional biochar for advanced wastewater remediation: A review. *International Journal of Biological Macromolecules*, 331, 1, pp. 148331. https://doi.org/10.1016/j.ijbiomac.2025.148331

Dechapanya, W., & Khamwichit, A. (2023). Biosorption of aqueous Pb(II) by H_3PO_4-activated biochar prepared from palm kernel shells. *Heliyon*, 9, 7, e17250, pp. 1–12. https://doi.org/10.1016/j.heliyon.2023.e17250

Fanzhi, Q., Chen, Z., Guangming, Z., Danlian, H., Xiaofei, T., & Abing, D. (2022). Lignocellulosic biomass carbonization for biochar production and characterization of biochar reactivity. *Renewable and Sustainable Energy Reviews*, 157, 112056, pp. 1–14. https://doi.org/10.1016/j.rser.2021.112056

Gimba, C. E., Olayemi, J. Y., Okunnu, S. T., & Kagbu, J. A. (2001). Adsorption of methylene blue by activated carbon from coconut shell. *Global Journal of Pure and Applied Sciences*, 7, 2, pp. 265–268.

He, P., Li, Y., Yu, K., Yan, P., Liu, W., Zhang, M., & Ma, L. (2025). Hierarchical porous composite carbon microsphere superstructures based on d-p orbital hybridization for efficient capture of low-concentration Cs. *Small*, 21, 25, e2409054, pp. 1–10. https://doi.org/10.1002/smll.202409054

Huang, T., & Imran, I. (2025). Mitigating cadmium contamination in soil using biochar, sulfur-modified biochar, and other organic amendments. *International Journal of Phytoremediation*, 27, 6, pp. 874–887. https://doi.org/10.1080/15226514.2025.2454515

Ivan, K., & Iryna, Y. (2025). Impact of chemical and physical treatments on the structural and surface properties of activated carbon and hydrochar. *ACS Sustainable Chemistry & Engineering*, 13, 6, pp. 2500–2507. https://doi.org/10.1021/acssuschemeng.4c09189

Jui-Yen, L., Ingyu, L., Jing-Hua, T., Wanze, L., Hyunook, K., & Chin-Pao, H. (2023). The surface acidity of freshly synthesized microplastics particles in simple electrolyte. *Colloids and Surfaces A: Physicochemical and Engineering Aspects*, 675, 132000, pp. 1–10. https://doi.org/10.1016/j.colsurfa.2023.132000

Khandoker, S. S., Nitesh, K. K., Md. Ashiqur, R., Hasan, J., Youssef, H., Stephen, J. E., Alfred, D. F., Lokendra, P., & Lucian, A. L. (2023). Comparison and assessment of methods for cellulose crystallinity

determination. *Chemical Society Reviews*, 52, 18, pp. 6417–6446. https://doi.org/10.1039/D2CS00569G

Kumari, A., Yadav, M., Bhatia, A., Sharma, M., & Bhateria, R. (2025). A review and bibliometric analysis on recent modification of biochar for effective and sustainable remediation of heavy metals in aqueous medium. *Discover Chemical Engineering*, 5, 21, pp. 1–15. https://doi.org/10.1007/s43938-025-00088-7

Kun, W., Ziyao, C., Guanzhen, W., & Qing, Q. (2024). Rational design of amorphous nanomaterials for enhanced electrochemical CO_2 and nitrate reduction. *ChemCatChem*, 16, 17, e202400415, pp. 1–12. https://doi.org/10.1002/cctc.202400415

Kwon, C. W., Tae, S., & Mandal, S. (2025). Comparative analysis of CO_2 adsorption performance of bamboo and orange peel biochars. *Molecules*, 30, 7, pp. 1607–1618. https://doi.org/10.3390/molecules30071607

Masud, H., Yanju, L., Ravi, N., Jianhua, D., Fangjie, Q., Scott, W. D., & Md, M. I. (2021). Mesoporous biopolymer architecture enhanced the adsorption and selectivity of aqueous heavy-metal ions. *ACS Omega*, 6, 24, pp. 15316–15331.

Naifar, A., Oueslati, K., Lima, E. C., Aouaini, A., & Ben, L. A. (2025). In-depth study of captopril adsorption on a biosourced sorbent: Statistical physics approach and characterization with adsorption modeling. *Langmuir*, 41, 25, pp. 16115–16127. https://doi.org/10.1021/acs.langmuir.5c01235

Neme, I., Gonfa, G., & Masi, C. (2022). Activated carbon from biomass precursors using phosphoric acid: A review. *Heliyon*, 8, e11940, pp. 1–12. https://doi.org/10.1016/j.heliyon.2022.e11940

Nuñez-Vargas, D., Barraza-Burgos, J., Guerrero-Perez, J., Diaz, L., Dalai, A. K., & Borugadda, V. B. (2026). Oil palm shell-derived activated carbon: Adsorption kinetics, thermodynamics, and interaction mechanism for lufenuron pesticide. *ACS Omega*, 11, 5, pp. 7005–7013. https://doi.org/10.1021/acsomega.4c10096

Obey, G., Tirivashe, P. M., & Macdonald, T. M. (2024). Immobilization and adsorption mechanisms of agro-waste based biochar: Effectiveness of pyrolytic temperatures on heavy metal removal. *Environmental Chemistry and Ecotoxicology*, 6, pp. 92–103. https://doi.org/10.1016/j.enceco.2024.04.002

Padmaja, V. M., Richelle, M. R., Pei, L. Y., Dusan, L., & Mahaveer, D. K. (2024). Advances in high surface area porous materials for efficient removal of toxic metal ions from water. *Progress in Materials Science*, 146, 101314, pp. 1–20. https://doi.org/10.1016/j.pmatsci.2024.101314

Pan, J., Deng, H., Du, Z., Tian, K., & Zhang, J. (2022). Design of nitrogen-phosphorus-doped biochar and its lead adsorption performance. *Environmental Science and Pollution Research*, 29, 19, pp. 28984–28994. https://doi.org/10.1007/s11356-021-17335-3

Raji, Z., Karim, A., Karam, A., & Khalloufi, S. (2023). Adsorption of heavy metals: Mechanisms, kinetics, and applications of various adsorbents in wastewater remediation—A review. *Waste*, 1, 3, pp. 775–805. https://doi.org/10.3390/waste1030046

Rukayat, O. Q., Abiodun, O. A., Olushola, S. A., & Olayide, S. L. (2024). Conversion of palm kernel shell to sustainable energy and effect of wet synthesized iron nanoparticles on thermal degradation

kinetics. *Bioresource Technology Reports*, 27, 101933, pp. 1–10.

.

Availability of Data and Materials

The datasets used and/or analyzed during the current study are available from the corresponding author on reasonable request.

Competing Interest

The authors have no competing interests to declare that are relevant to the content of this article.

Funding Declaration

This research did not receive funding.

Author contributions

All authors contributed to the study conception of this research. Conceptualization: [Idowu J. Esho, Emmanuel F. Olasehinde and Matthew A. Adebayo]; Methodology: [Idowu J. Esho]; Formal analysis and investigation: [Idowu J. Esho, Emmanuel F. Olasehinde and Matthew A. Adebayo]; Writing - original draft preparation: [Idowu J. Esho and Matthew A. Adebayo]; Writing - review and editing: [Idowu J. Esho, Emmanuel F. Olasehinde and Matthew A. Adebayo]; Supervision: [Emmanuel F. Olasehinde and Matthew A. Adebayo]